

Electronic Supplementary Information

The multiple roles of carbonic anhydrase in calcium carbonate mineralization

Carlos Rodriguez-Navarro,^{a*} Özlem Cizer,^b Krzysztof Kudłacz,^c Aurelia Ibañez-Velasco,^a Cristina Ruiz-Agudo,^d Kerstin Elert,^a Alejandro Burgos-Cara,^a and Encarnacion Ruiz-Agudo^a

¹Department of Mineralogy and Petrology, University of Granada, Fuentenueva s/n, 18002 Granada, Spain.

²Department of Civil Engineering, KU Leuven, Kasteelpark Arenberg 40 B-3001 Heverlee, Belgium.

³CODEGOPL, Rydlówka 42A/13, 30-363 Kraków, Poland.

⁴Physical Chemistry, University of Konstanz, Universitätsstraße 10, 78457 Konstanz, Germany.

*Corresponding author e-mail: carlosrn@ugr.es

Content:

Fig. S1. Optical microscopy micrographs of precipitates formed at the air-solution interface in the presence of 1.5 μM CA

Fig. S2. Optical microscopy micrograph and corresponding μ -Raman spectra of solids formed during droplets carbonation in the presence of 1.5 μM CA

Fig. S3. FESEM images of the nanogranular surface structure of calcite crystals formed in the presence of 1.5 μM CA.

Fig. S4. ESEM photomicrographs and EDS spectra of precipitates formed in the presence of 1.5 μM CA.

Fig. S5. Characterization of pure CA

Fig. S6. Circular dichroism (CD) spectra of 5 μM CA solutions.

Fig. S7. TEM images of CA supramolecular structures.

Fig. S8. TEM-HAADF imaging and EDS maps of CA aggregates formed during calcium potentiometric titration experiments.

Fig. S9. TEM image of CA observed after drying of an aqueous solution of the pure enzyme.

Fig. S10. In situ transformation of anhydrous ACC in the TEM.

Supplementary Figures

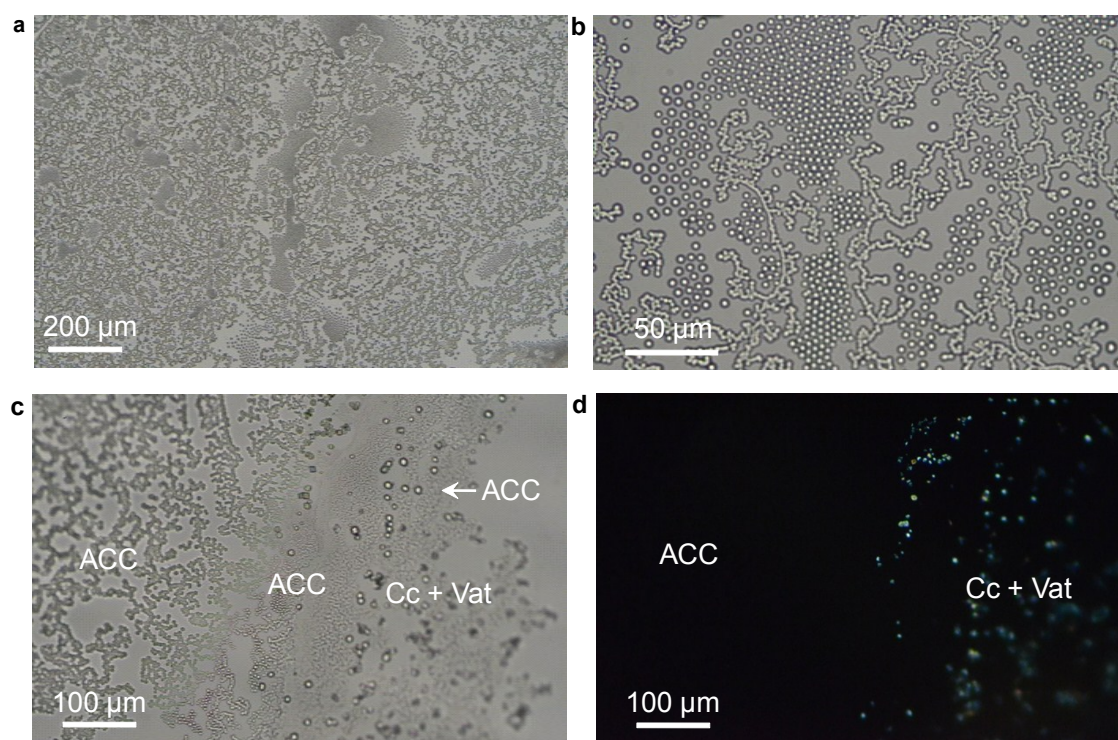


Fig. S1. Optical microscopy micrographs of precipitates formed at the air-solution interface in the presence of 1.5 μM CA. (a) General view of the air-solution interface right after droplet exposure to atmospheric CO₂. **(b)** Detail of **(a)** showing individual spherical ACC particles as well as ACC fractal aggregates. **(c)** Advancement (from the right to the left) of the ACC to crystalline transformation front via dissolution of ACC and precipitation of calcite (Cc) and vaterite (Vat) crystals. **(d)** crossed-polars image of the area depicted in **(c)** demonstrating the amorphous nature of ACC precipitates (on the left) and the birefringence of crystalline calcite and vaterite precipitates (on the right).

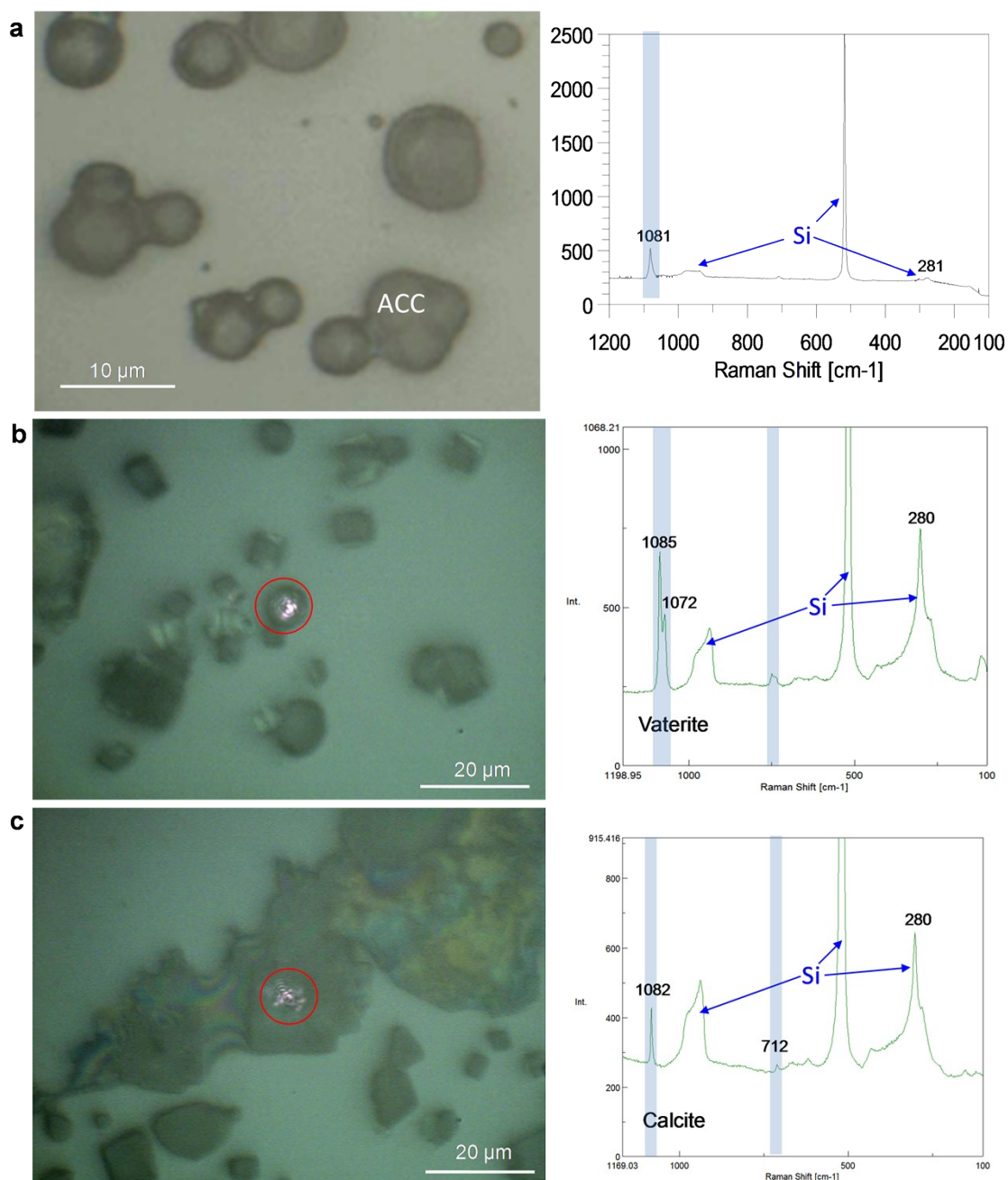


Fig. S2. Optical microscopy micrograph and corresponding μ -Raman spectra of solids formed during droplets carbonation in the presence of $1.5 \mu\text{M}$ CA. (a) ACC formed after 10 min, presumably poorly hydrated. Vaterite (b) and calcite (c) formed after 30 min air exposure. The red circles mark the areas analyzed by μ -Raman. Shaded bars mark the bands corresponding to the carbonate phases, whereas the non-shaded bands correspond to the Si wafer.

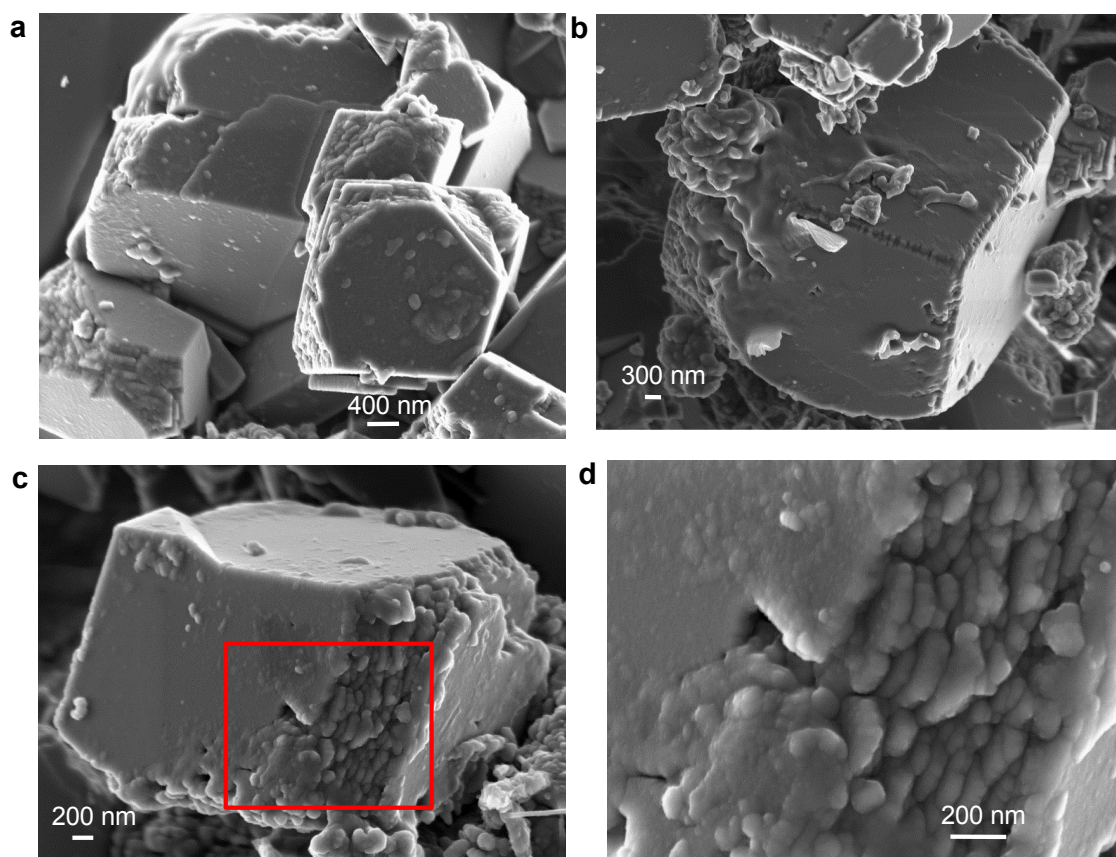


Fig. S3. FESEM images of the nanogranular surface structure of calcite crystals formed in the presence of 1.5 μM CA. (a) General overview of calcite crystals with rounded edges limited by macrosteps (a detail of this image is shown in Fig. 2e). (b) Calcite rhombohedron with rounded edges in one side and straight edges on the other side, with grooves lined with nanoparticles (a detail of this image is shown in Fig. 2d). (c) Another example of calcite rhombohedron with roughened, stepped faces. (d) detail of the red-squared area in (c) showing the nanogranular structure.

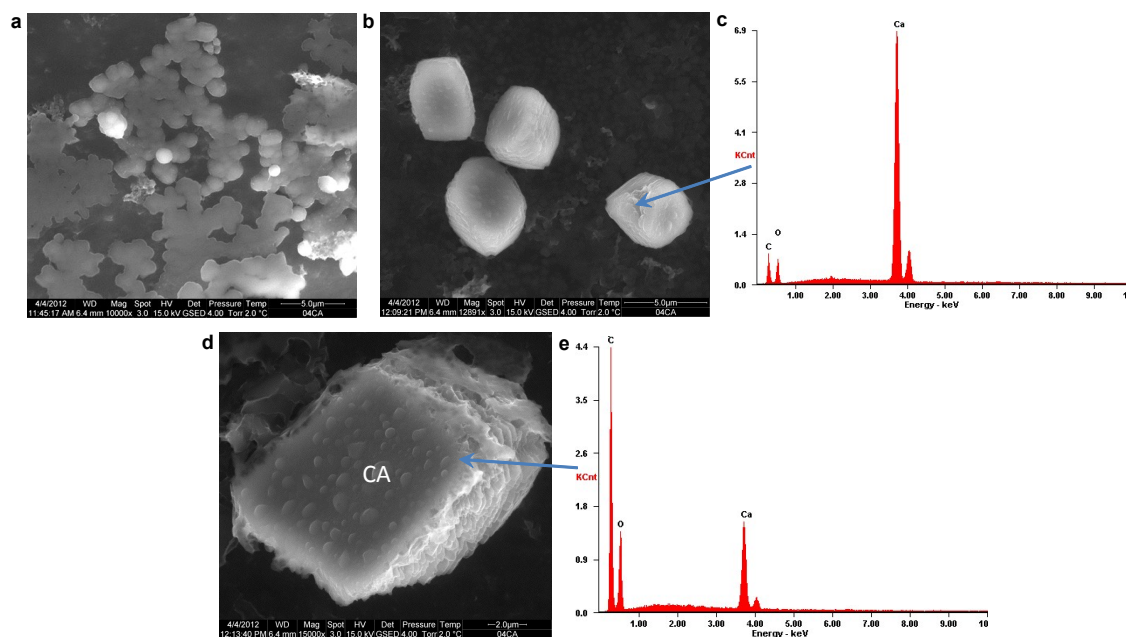


Fig. S4. ESEM photomicrographs and EDS spectra of precipitates formed in the presence of 1.5 μ M CA. (a) ACC nanoparticle aggregates formed at the droplet air-solution interface. **(b)** Calcite rhombohedra with rounded edges and stepped faces, partially/fully covered by CA films. **(c)** EDS spectrum of the arrowed calcite crystal in **(b)**, which does not show CA film covering on the analyzed spot. **(d)** Calcite rhombohedron with a CA film. A detail of this calcite-CA hybrid is shown in Fig. 2h. **(e)** EDS spectrum of the arrowed point in the calcite crystal covered by CA in **(d)**. Note the higher C content (i.e., higher C peak) in this spectrum as compared with that of the bare area of calcite shown in **(c)**.

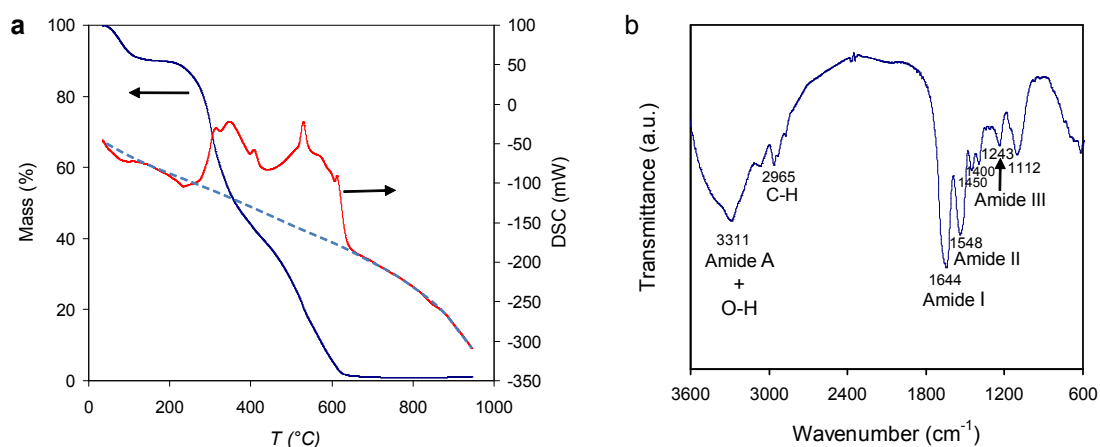


Fig. S5. Characterization of pure CA. (a) TG and DSC, showing and initial weight loss (25-160 °C) corresponding to H₂O loss, associated with an endothermic band, followed by a two-step exothermic oxidation event (200-650 °C) resulting in complete decomposition (the dashed blue line marks the background for the DSC trace). (b) FTIR spectrum showing the bands corresponding to N-H stretch of amide A plus O-H stretching (3311 cm⁻¹), C-H bending (2965 cm⁻¹), C=O stretching of amide I and carboxylic groups (~1644 cm⁻¹), and N-H bending of amide II (1548 cm⁻¹). Bands at lower wavenumbers correspond to the amide III region.

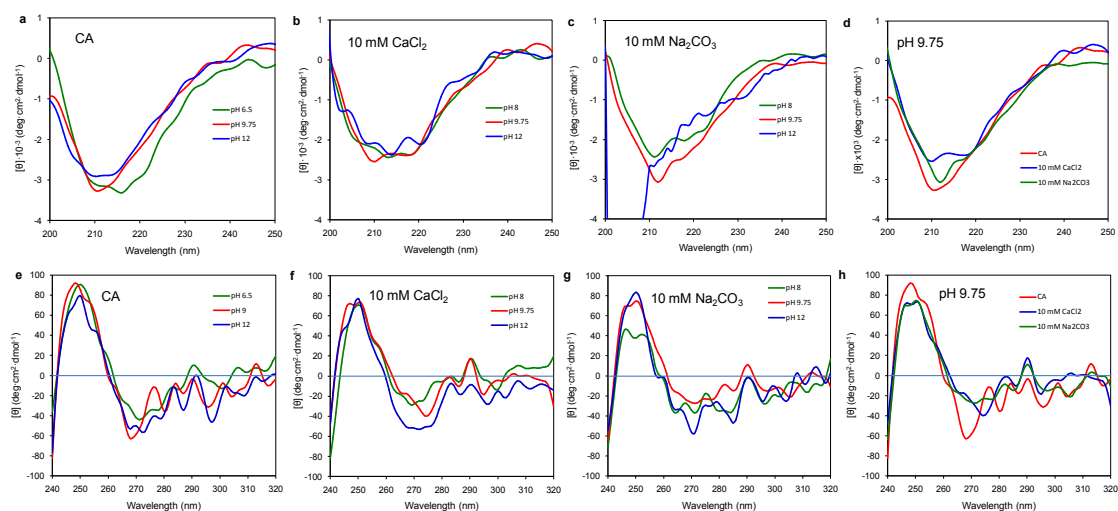


Fig. S6. Circular dichroism (CD) spectra of 5 μ M CA solutions. (a) Far-UV CD of pure enzyme solutions at different pHs. (b) Far-UV CD of enzyme solution dosed with 10 mM CaCl_2 at different pHs. (c) Far-UV CD of enzyme solutions dosed with 10 mM Na_2CO_3 at different pHs. (d) Far-UV CD of enzyme solution with and without 10 mM CaCl_2 or 10 mM Na_2CO_3 at pH 9.75. (e) Near-UV CD of pure enzyme solutions at different pHs. (f) Near-UV CD of enzyme solution dosed with 10 mM CaCl_2 at different pHs. (g) Near-UV CD of enzyme solutions dosed with 10 mM Na_2CO_3 at different pHs. (h) Near-UV CD of enzyme solution with and without 10 mM CaCl_2 or 10 mM Na_2CO_3 at pH 9.75. All spectra collected after 60 min incubation time.

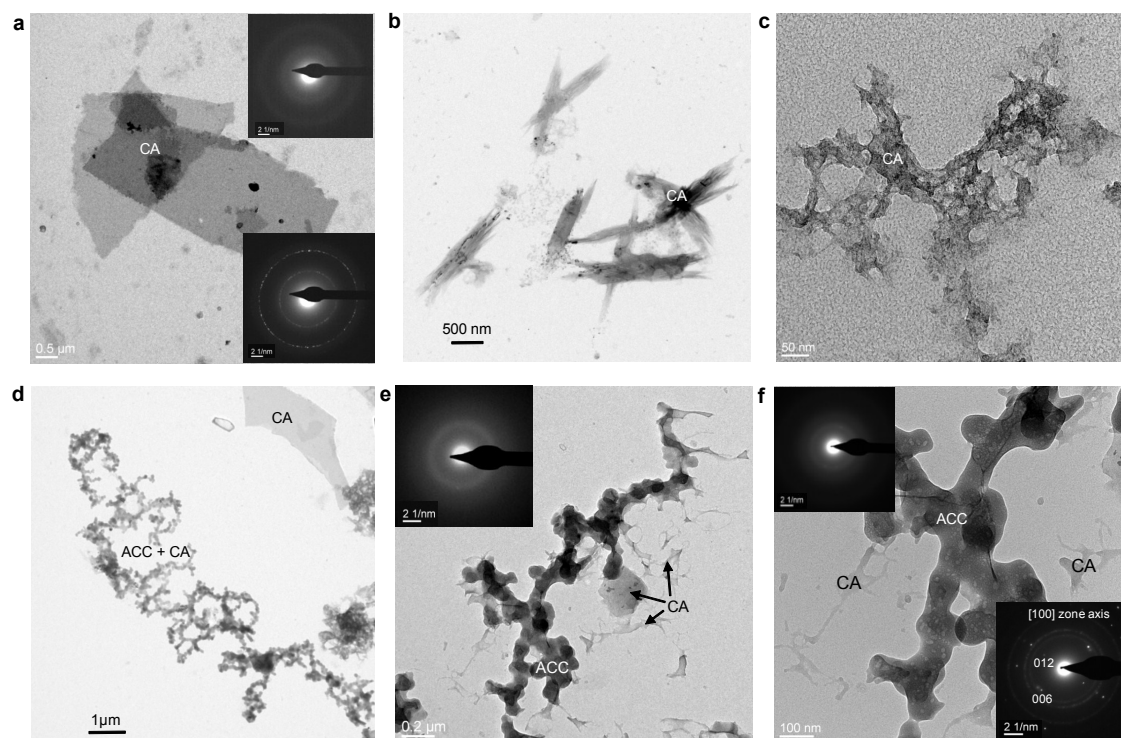


Fig. S7. TEM images of CA supramolecular structures. (a) CA sheets in solutions collected during Stage II. The upper and lower insets show SAED patterns of the CA sheets before and after 30 s focused e-beam irradiation, respectively. (b) Aggregates of CA formed during the post-nucleation stage during calcium potentiometric titration tests. (c) Hydrogel-like aggregate of CA formed during Stage II. (d) Film-like, fibrous and hydrogel-like aggregates of CA partially mineralized by ACC (Stage II). (e) Detail of CA structures in (d) with attached anhydrous ACC (SAED pattern in inset). (f) High magnification detail of the red-squared area in (e) showing anhydrous ACC associated with CA fibrils. The upper left and lower right insets show the SAED pattern of anhydrous ACC before and after 30 s focused e-beam irradiation, respectively. Note that the irradiated structure corresponds to oriented calcite corroborating that the ACC was anhydrous.

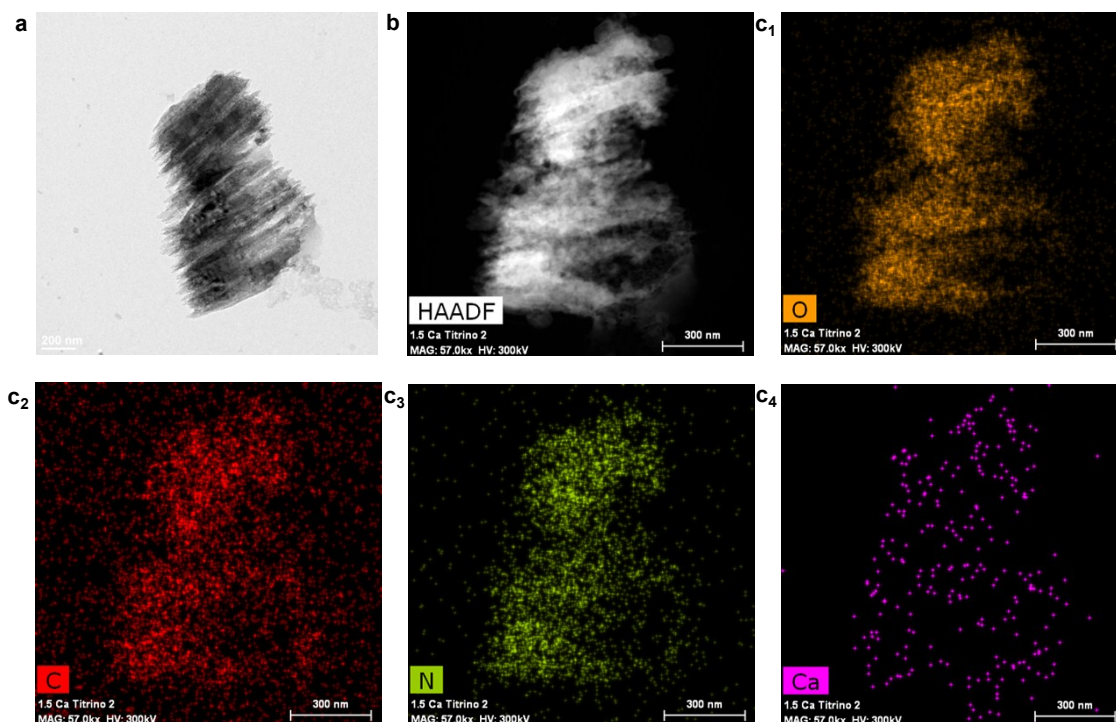


Fig. S8. TEM-HAADF imaging and EDS maps of CA aggregates formed during calcium potentiometric titration experiments. (a) Bright field TEM image of protein sheet-like aggregates (observed edge-on). (b) HAADF image of the aggregate in (a). (c₁-c₄) EDS elemental maps of the CA aggregates in (b). Note the significant amount of N confirming that these are protein structures. Note also the negligible amount of Ca in the CA structure, consistent with the lack of significant complexation of calcium by the protein shown by our calcium potentiometric titration tests.

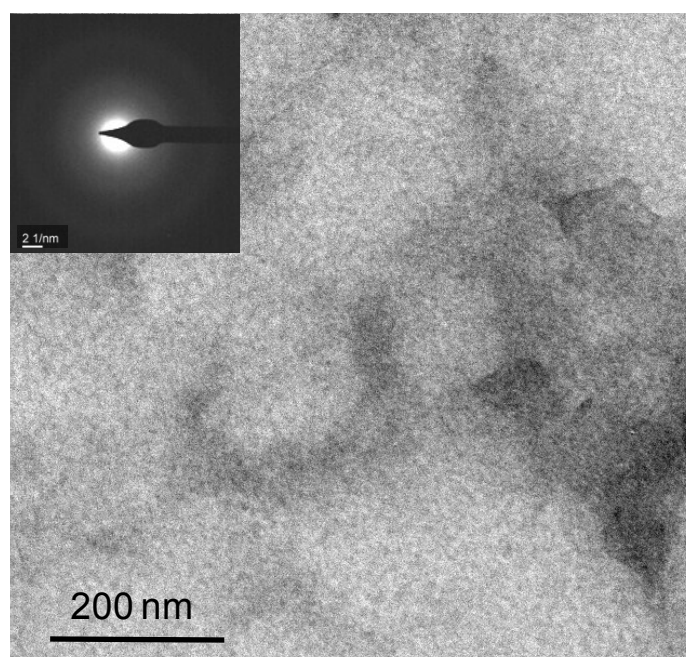


Fig. S9. TEM image of CA observed after drying of an aqueous solution of the pure enzyme.

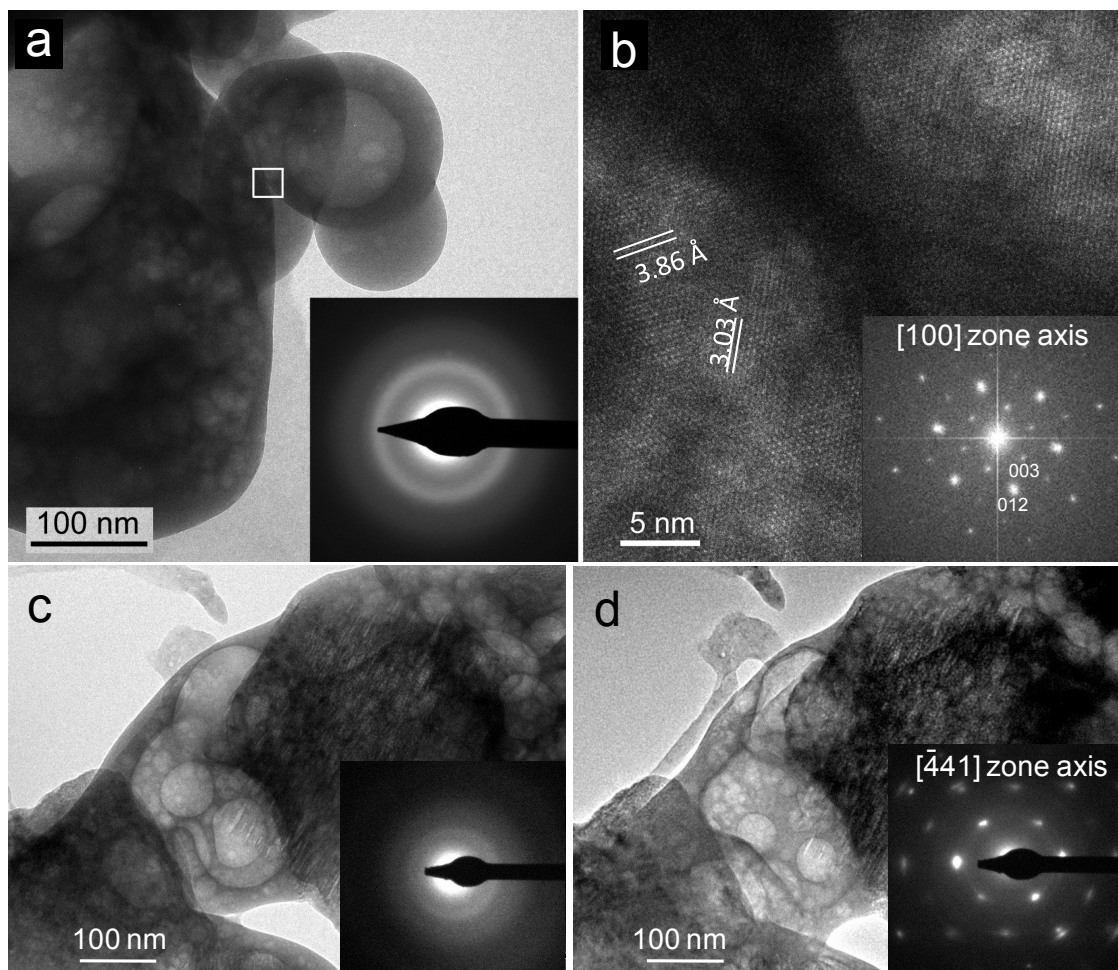


Fig. S10. In situ transformation of anhydrous ACC in the TEM. (a) TEM photomicrograph and SAED (inset) of an aggregate of anhydrous ACC formed in the presence of 1.5 μM CA. (b) HRTEM photomicrographs of the squared area in (a) after transformation into calcite following focused e-beam exposure for 30 s. The lattice fringes show formation of oriented calcite as confirmed by the FFT image (inset) showing the $[42\bar{1}]$ orientation of the aggregate. The orientation and d-spacing of $(104)_{\text{calcite}}$ and $(012)_{\text{calcite}}$ are indicated. (c) Anhydrous ACC before focused e-beam exposure (SAED pattern in inset). (d) the same anhydrous ACC aggregate in (c) after 30 s focused e-beam exposure showing negligible shrinking and resulting single-crystal calcite (SAED pattern in inset).